PROCEEDINGS OF SCIENCE

Hydrodynamics and instabilities of relativistic astrophysical jets in AGN

I.P. van der Westhuizen*, **B. van Soelen, P.J. Meintjes**
Department of Physics, University of the Free State, 9301, RSA
vanderwesthuizenip@ufs.ac.za

J.H. Beall

St. John's College, Annapolis, MD, 21401, USA

Active galactic nuclei (AGN) show variability over both intra day and longer time scales. This characteristic has been the topic of many recent studies especially the investigation of correlation between multi-wavelength components. The variability can be investigated through numerical hydrodynamics. In this study an ideal relativistic hydrodynamic jet was simulated in order to investigate the instabilities which form in the jet as a source of variability in AGN. A synchrotron delta-approximation model was applied to the hydrodynamical environment in order to obtain an estimate of the intensity emitted at an example frequency of 15 GHz. This frequency was chosen such that the estimated intensity maps could be comparable to radio observational surveys. The tools used in such a hydrodynamic model can be applied to other transient sources such as X-ray binaries which have been shown to produce jet-like components.

Frontier Research in Astrophysics — II
23-28 May 2016
Mondello (Palermo), Italy

*Speaker.

PoS(FRAPWS2016)081

1. Introduction

Radio observations of Active Galactic Nuclei (AGN) have shown that many of these sources produce extended radio emission associated with relativistic jet-like outflows. These radio jet-like structures consist of a narrow beam of material being ejected from the nucleus of the host galaxy, which can extend up to megaparsec scale distances. Radio loud AGN containing relativistic jets produce emission over a large range of the electromagnetic spectrum and the spectral energy distribution of such sources have a characteristic double bump structure. The emission in the lower bump is mainly produced through synchrotron radiation of relativistic electrons spiralling in the magnetic field of the jet, while the high energy component may be due to a mixture of inverse-Compton scattering of the synchrotron radiation, as well as external photons and hadronic processes (see e.g. [1, 2]).

The emission characteristics of AGN make them ideal targets for multi-wavelength studies. High resolution radio observations, conducted by the VLBI, revealed that relativistic jets have complex internal structures and long term radio monitoring programs such as the MOJAVE (15 Ghz frequency band) [3, 4] and RRFID (8 and 2 GHz bands) surveys [5] have been undertaken to study the time dependent nature of the morphology of these jets. These studies have shown the presence of stationary as well as superluminal emission components travelling at apparent velocities on the order of $15c$, time dependent jet bending and changes in the injection angle of the jet (see e.g. [4]).

To investigate the morphology and instabilities that form inside these jets the macroscopic flow of such systems can be modelled by fluid dynamics. The complex nature of such a dynamic environment means that we will not be able to obtain an analytical solution, instead we turn to numerical methods in order to create an appropriate model of the system. Previous studies in the field of numerically modelling relativistic jets have investigated jet instabilities, shock propagation in jets and the influence of magnetic fields on the dynamic structure of the system (see e.g. [6, 7, 8]). In order to compare a numeric fluid dynamical simulation to observational data we have to calculate the emission based on an emission model. This model calculates the radiation that would be produced in the environment based on physical properties such as the energy and particle density in the system (see e.g. [9]).

In this paper we present a numeric fluid dynamical simulation containing an ideal relativistic jet propagating through a uniform ambient medium. The simulation was designed and evolved with time using the grid based numerical hydrodynamical code PLUTO [10]. This simulation is constructed under the assumption that the energy in the jet is kinetically dominated, with the magnetic field having negligible effects on the dynamic morphology of the jet. An emission model, in the form of a post-processing code, was applied to the simulation to generate approximate intensity maps of the synchrotron radiation produced by the environment. The synchrotron radiation was calculated at 15 GHz. This was done in order to compare the emission structures that have been observed in radio observations to those generated by the fluid dynamical simulation. Further details of the numeric fluid dynamical simulation are given in section 2 while the calculation of the intensity maps is discussed in section 3. Section 4 contains our results followed by a conclusion in section 5.

Parameter		Value (arbitrary units)
Lorentz factor	Γ	10
Velocity	v	$0.995c$
Density ratio	η	10^{-5}
Jet density	ρ_b	0.1
Ambient density	ρ_{am}	100
Mach number	M_b	7.8
Adiabatic index	γ_{ad}	$5/3$
Pressure	P	0.001

Table 1: Parameters used in the set up of the initial conditions.

2. Numeric fluid dynamical model

Grid based numeric fluid dynamical simulations consist of a set of defined cells in a mesh grid with assigned properties, such as density, velocity and energy, that adhere to the fluid dynamical conservation laws. The properties of each cell can be evolved with time according to a set of partial differential conservation equations in the form of,

$$\frac{\partial \vec{U}}{\partial t} = -\nabla \cdot \vec{\vec{T}}(\vec{U}) + \vec{S}(\vec{U}), \tag{2.1}$$

where $\vec{U}$ is a vector containing the conserved properties, $\vec{\vec{T}}(\vec{U})$ is a tensor containing flux vectors calculated between adjacent cells, as a function of $\vec{U}$, and $\vec{S}(\vec{U})$ comprises of source terms that account for effects such as gravity, the viscosity and resistivity of the fluid (see e.g. [11]).

The numerical model presented in this paper was set up in the relativistic hydrodynamic (RHD) regime with no source terms to simulate the production of an ideal relativistic fluid jet. The components of equation (2.1) in the RHD regime can be given as,

$$\vec{U} = \begin{bmatrix} \rho\Gamma \\ \rho\Gamma^2 h\mathbf{v} \\ \rho\Gamma^2 h - P \end{bmatrix}, \quad \vec{\vec{T}}(\vec{U}) = \begin{bmatrix} \rho\Gamma\mathbf{v} \\ \rho\Gamma^2 h\mathbf{v}\mathbf{v} + P\mathbf{I} \\ \rho\Gamma^2 h\mathbf{v} \end{bmatrix}^T, \quad \vec{S}(\vec{U}) = 0, \tag{2.2}$$

where ρ is the mass density in the co-moving frame, P is the pressure, h is the specific enthalpy, Γ is the bulk-flow Lorentz factor, $\mathbf{I}$ is a 3x3 unit matrix and $\mathbf{v}$ is the three velocity [10].

The simulation was set-up on a Cartesian mesh grid consisting of $64 \times 64 \times 128$ length units with a resolution of 4 points per unit length, resulting in $256 \times 256 \times 512$ computational cells. A uniform background medium was assigned to the grid with the initial z boundary set up to inject jet material through a nozzle of radius 1 into the environment. The less dense jet material was injected at a constant rate with a Lorentz factor $\Gamma = 10$. All other boundary conditions were set-up as outflow. The properties assigned to the ambient and jet material are listed in table 1. All units listed in table 1 are arbitrary except for the velocity which is given in units of the speed of light c. A pressure matched jet model was used for the simulation to ensure that the jet remained collimated at the injection site.

The numerical simulation was set-up and evolved with time using the open-source code PLUTO *ver* 4.2 [10]. The code uses upwind high resolution shock capturing algorithms to solve the conservation equations and evolve them with time. The set-up used piecewise parabolic interpolation, to determine the flux functions between cells, the HLLC Riemann solver and characteristic time stepping to evolve the properties of each cell with time [12]. The simulation was run until the head of the jet material reached the edge of the computational domain.

3. Artificial intensity maps

To construct artificial synchrotron intensity maps of the three dimensional simulation we first determined the radiation that will be emitted and absorbed by each cell. This was done by calculating the synchrotron emission and absorption coefficients based on the properties of the cell. In order to produce two dimensional intensity plots of the synchrotron radiation in the jet, the coefficients can be used to calculate the change in intensity through each cell along a line of sight s. The change in intensity (in the co-moving reference frame) can be given as,

$$\frac{dI_\nu}{ds} = j_\nu^{sy} - \alpha_\nu^{sy} I_\nu, \tag{3.1}$$

where the superscript "sy" indicates that the coefficients are calculated for synchrotron radiation [13].

The emission coefficient produced by synchrotron radiation is calculated by integrating the power radiated by a single radiating particle, $P_\nu(\gamma)$, over the particle spectrum $n(\gamma)$ of the medium [13],

$$j_\nu^{sy} = \frac{1}{4\pi}\int n(\gamma) P_\nu^{sy}(\gamma)\mathrm{d}\gamma. \tag{3.2}$$

Integrating the full expression for the radiative power of each cell in the computational domain can be very computationally intensive and to compensate for this the synchrotron radiative power was approximated using an analytical δ-function model [13]. The δ-function approximates the synchrotron power emitted by a particle of energy γ assuming that the particle only radiates at a critical frequency ν_c, given by,

$$\nu_c = \frac{3qB}{4\pi mc}\gamma^2. \tag{3.3}$$

The expression for the radiative power of the δ-function approximation is given by,

$$P_\nu^{sy,\delta}(\gamma) = \frac{32\pi}{9}\left(\frac{q^2}{mc^2}\right)^2 u_B \beta^2 c \gamma^2 \delta(\nu - \nu_c), \tag{3.4}$$

where q is the charge of the radiating particle, m is the mass of the radiating particle, c is the speed of light, u_B is the magnetic field energy density and ν is the frequency of emission in the co-moving frame [13].

In our calculation we assumed that the dominant radiative particles in the jet consisted of non-thermal electrons with a power-law particle distribution given by,

$$n(\gamma) = n_0 \gamma^{-p}, \tag{3.5}$$

where the normalization factor, n_0, is determined by [14]

$$n_0 = \left(\frac{e(p-2)}{1-C_E^{2-p}}\right)^{p-1}\left(\frac{1-C_E^{1-p}}{\frac{\rho}{m_p}(p-1)}\right)^{p-2}. \tag{3.6}$$

Here m_p is the mass of a proton, p is the power-law index, e is the internal energy density and C_E is the ratio of the maximum and minimum energies. For our initial estimates we chose $p = 1.8$ and $C_E = 10^3$. The internal energy density of the system can be calculated using the caloric equation of state [15],

$$e = \frac{P}{\rho(\gamma_{\text{ad}} - 1)}, \tag{3.7}$$

in which γ_{ad} is the adiabatic index of the fluid. The magnetic field energy density is assumed to be an equipartition fraction of the internal energy density calculated as,

$$u_B = \varepsilon_B e \tag{3.8}$$

where $\varepsilon_B = 10^{-3}$ was used based on values given by [16].

Combining the previous expressions (3.3-3.7) and integrating equation (3.2) we obtain an expression for the emissivity,

$$j_\nu^{sy} = \frac{4}{9}\left(\frac{q^2}{mc^2}\right)^2 u_B \nu^{\frac{1}{2}} \nu_0^{\frac{-3}{2}} \beta^2 cn\left(\sqrt{\frac{\nu}{\nu_0}}\right), \tag{3.9}$$

where,

$$\nu_0 = \frac{3qB}{4\pi mc}. \tag{3.10}$$

A similar analysis was applied to the absorption coefficient, where the absorption coefficient was calculated as,

$$\alpha_\nu^{sy} = -\frac{1}{8\pi m\nu^2}\int P_\nu^{sy,\delta}(\gamma)\gamma^2 \frac{\partial}{\partial\gamma}\left(\frac{n(\gamma)}{\gamma^2}\right)\mathrm{d}\gamma, \tag{3.11}$$

which leads to the expression,

$$\alpha_\nu^{sy} = \frac{2}{9}\frac{p+2}{m\nu^2}\left(\frac{q^2}{mc^2}\right)^2 u_B \nu_0^{-1} \beta^2 cn\left(\sqrt{\frac{\nu}{\nu_0}}\right). \tag{3.12}$$

A detailed description of this derivation can be found in [13].

Before the coefficients are used to calculate the two dimensional intensity map, Lorentz transformations must be applied to move from the co-moving to the stationary reference frame of the galaxy. This effect is due to the relativistic velocity of the bulk flow in the simulation. The synchrotron coefficients of each cell transform as,

$$j_\nu^{sy} = \frac{j_{\nu'}^{sy\prime}}{(\Gamma[1-\beta\mu])^2}, \tag{3.13}$$

$$\alpha_\nu^{sy} = \alpha_{\nu'}^{sy\prime}(\Gamma[1-\beta\mu]) \tag{3.14}$$

where the primed terms indicate quantities calculated in the co-moving reference frame, the unprimed quantities are in the galactic stationary frame, and μ is the cosine of the angle between the

observer and the velocity of the fluid in the galactic stationary frame [13].For our initial calculations we assumed that the radiative losses are negligible when compared to the total energy of the injected jet material (see [9] for a discussion including radiative losses), and additional effects such as the light travel time and the expansion of the universe were also neglected.

The two dimensional intensity maps were computed using a post-processing code written in the Python programming language. In this code the user can arbitrarily set the line of sight s for integration as well as the frequency of the intensity maps in the stationary frame. The frequency set by the user in the stationary frame is transformed to the co-moving frame of each cell in the code before the coefficients are calculated. The intensity is then integrated along the set line of sight to create a two dimensional intensity map.

4. Results

The numerical simulation was run with the set-up and parameters as discussed in section 2. Figure 1 illustrates plots of xz-slices containing the density, pressure and velocity magnitude distributions for the environment, as well as the corresponding calculated intensity map, calculated at the 15 GHz frequency, for the same time step.

We note the formation of 5 distinct regions within these plots of the simulation. Firstly the outer uniform region consists of the background material initially assigned to the cells. As jet material is injected into the environment, at supersonic speeds through the nozzle on the initial z boundary, it compresses the background material and forms a terminal bow shock surrounding the body of the jet. This terminal bow shock propagates through the ambient medium forming a region of turbulent high pressure material. In the central region we obtain a relativistic beam of jet material. Close to the injection site this beam is very stable, highly collimated and shows little deceleration (as shown in figure 1(c)). Instabilities grow larger as the distance from the injection site increases creating bends in the beam at 40 length units and breaking apart the beam at a distance of 85 units.

At the head of the beam, the region between the jet and the high pressure shocked material forms a shock front, referred to as the working surface. At this surface the remaining kinetic energy of the injected jet medium is converted into internal energy which creates a hot spot of emission on the intensity map in figure 1(d). This interaction at the working surface also drives a backflow of material, which forms a cocoon around the central beam and limits further interaction between the jet and background medium. This cocoon assists in the collimation of the beam and prevents further deceleration of the jet material [15].

Plotting the density along the center of the beam in the z-direction (as shown in figure 2) we note the occurrence of harmonic oscillations in these properties close to the injection nozzle. These oscillations form stationary shock fronts in the beam, called re-collimation shocks, and are caused by the over-pressured shocked medium acting on the beam. This is also illustrated in figure 1(b). As the material propagates further from the injection site these shocks are damped and the beam becomes more unstable. At a distance of 40 length units the beam transitions from being re-collimation shock dominated to a turbulent regime. The turbulence forms due to hydrodynamic instabilities caused by the interaction between the beam of the jet and the surrounding cocoon region. Figure 2 also shows the working surface at a distance of 105 units.

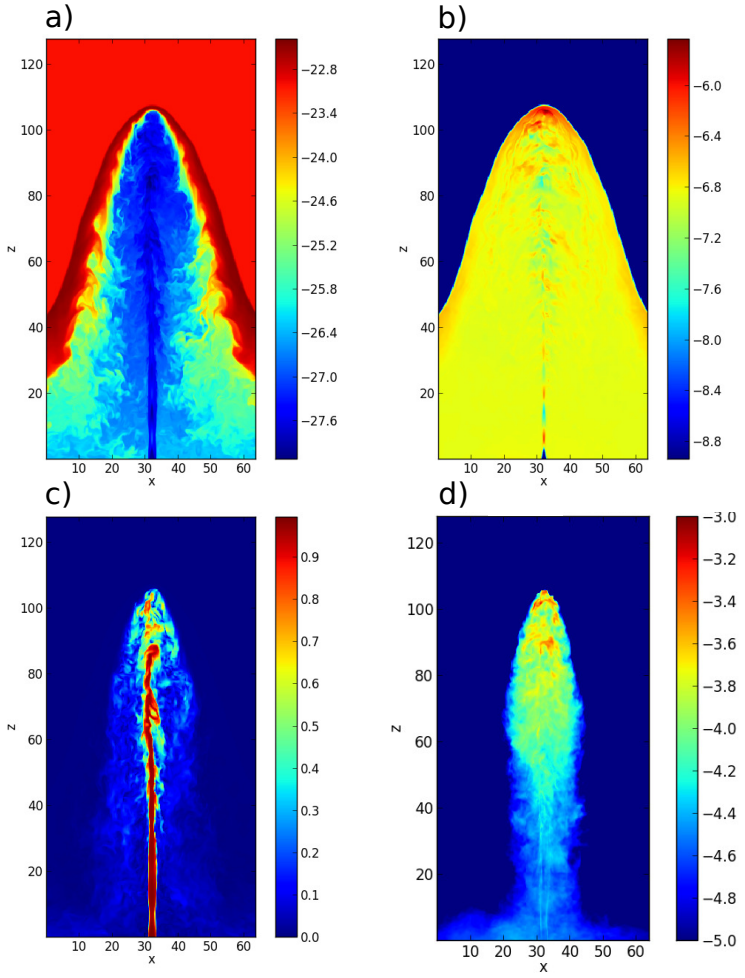

Figure 1: Visualization of the simulation results showing a) the density slice through the *xz*-plane of the jet b) the pressure slice through the *xz*-plane of the jet, c) the velocity magnitude slice through the *xz*-plane of the jet and d) the calculated intensity map at 15 GHz. Logarithmic scales are shown for the density and pressure plots in arbitrary units, while the velocity plots have a linear scaling in units of c. The intensity map is map is scaled as the logarithm of arbitrary units.

To determine what effect these structures have on the synchrotron radiation the emission and absorption coefficients were calculated according to equations (3.9) and (3.12) for a frequency of 15 GHz. The synchrotron intensity maps calculated from the hydrodynamic simulation will allow the structures in the simulation to be compared to observational data at a later stage. Figure 3 shows a three dimensional rendering of the trace of injected jet material with the colour indicating the emission coefficient.

This rendering shows that the emission close to the injection nozzle is dominated by the beam of the jet with the presence of faintly emitting material in the cocoon. As the distance from the

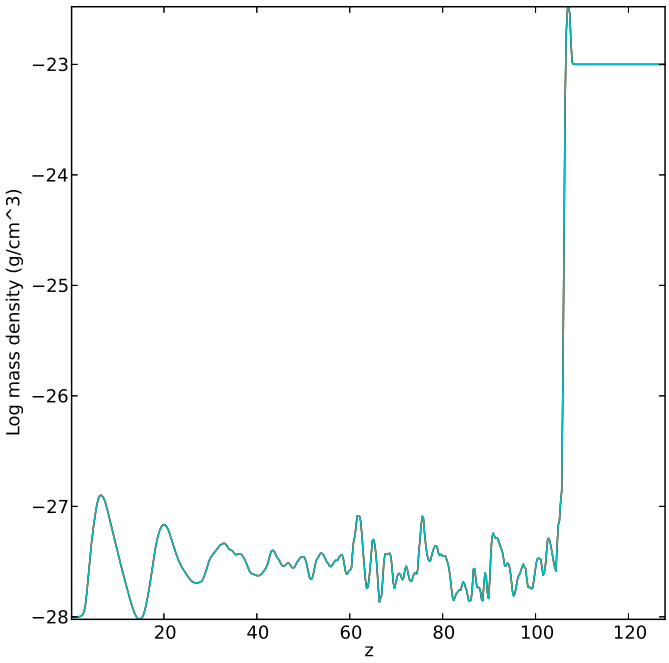

Figure 2: One dimensional plot of the density through the central beam.

injection site increases we note that the cocoon becomes the dominant emission region forming a lobe type structure at the head of the jet. Hotspots can be seen on the head of the cocoon due to the conversion of energy by the working surface.

To calculate intensity maps we considered a jet propagating perpendicular with respect to an observer. Figure 4 shows the variation in emission and hot spot regions in sequential time steps. These results show that even though a constant injection rate was applied to the jet material variability can occur in the intensity maps. This variability is attributed to the occurrence of turbulence in the beam at large distances from the injection nozzle.

5. Conclusion

In this paper we were able to recreate an ideal relativistic jet environment using the PLUTO hydrodynamic code. The results show the formation of a collimated relativistic beam with little deceleration surrounded by a cocoon region of backflowing material. These results are in accordance with previous studies such as [8, 15].

The results show that the internal structure of the beam is initially dominated by re-collimation shocks but transitions to a turbulent regime further from the injection site. Estimates of the synchrotron emission generated by such a jet has shown large scale similarities to FRII type radio galaxy structures with a relativistic beam, a lobe structures at the head of the jet as well as hot spots on the lobes.

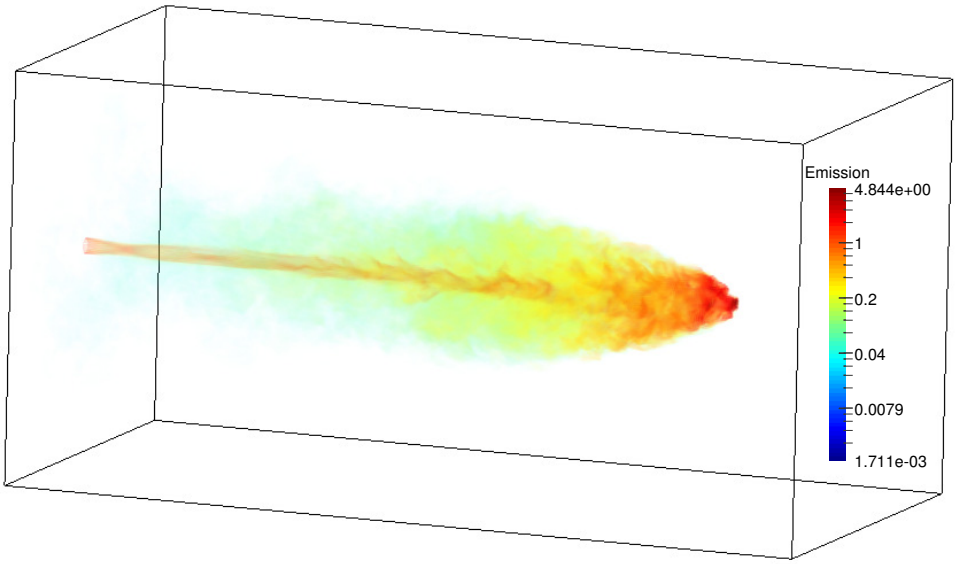

Figure 3: Three dimensional rendering of the emission coefficient of the jet material.

In order to make an accurate quantitative comparison between the simulation results and observational data more complex effects must be taken into account. These include effects such as gravity and viscosity in the fluid dynamical simulations, the cosmological expansion, time of arrival effects as well as a change in the particle spectrum within the jet.

Simulations such as the one presented in this paper are not limited to sources such as AGN. Many other sources such as microquasars and γ-ray bursts (GRB) have been associated with the production of jets and the resulting synchrotron radiation.

Acknowledgments

Acknowledgement is given to the HPC unit at the University of the Free State for their assistance in the installation and set up of software used to run simulations on the UFS HPC.
The financial assistance of the National Research Foundation (NRF) towards this research is hereby acknowledged. Opinions expressed and conclusions arrived at, are those of the author and are not necessarily to be attributed to the NRF. This work is based on the research supported in part by the National Research Foundation of South Africa for the grant 87919. Any opinion, finding and conclusion or recommendation expressed in this material is that of the authors and the NRF does not accept any liability in this regard.

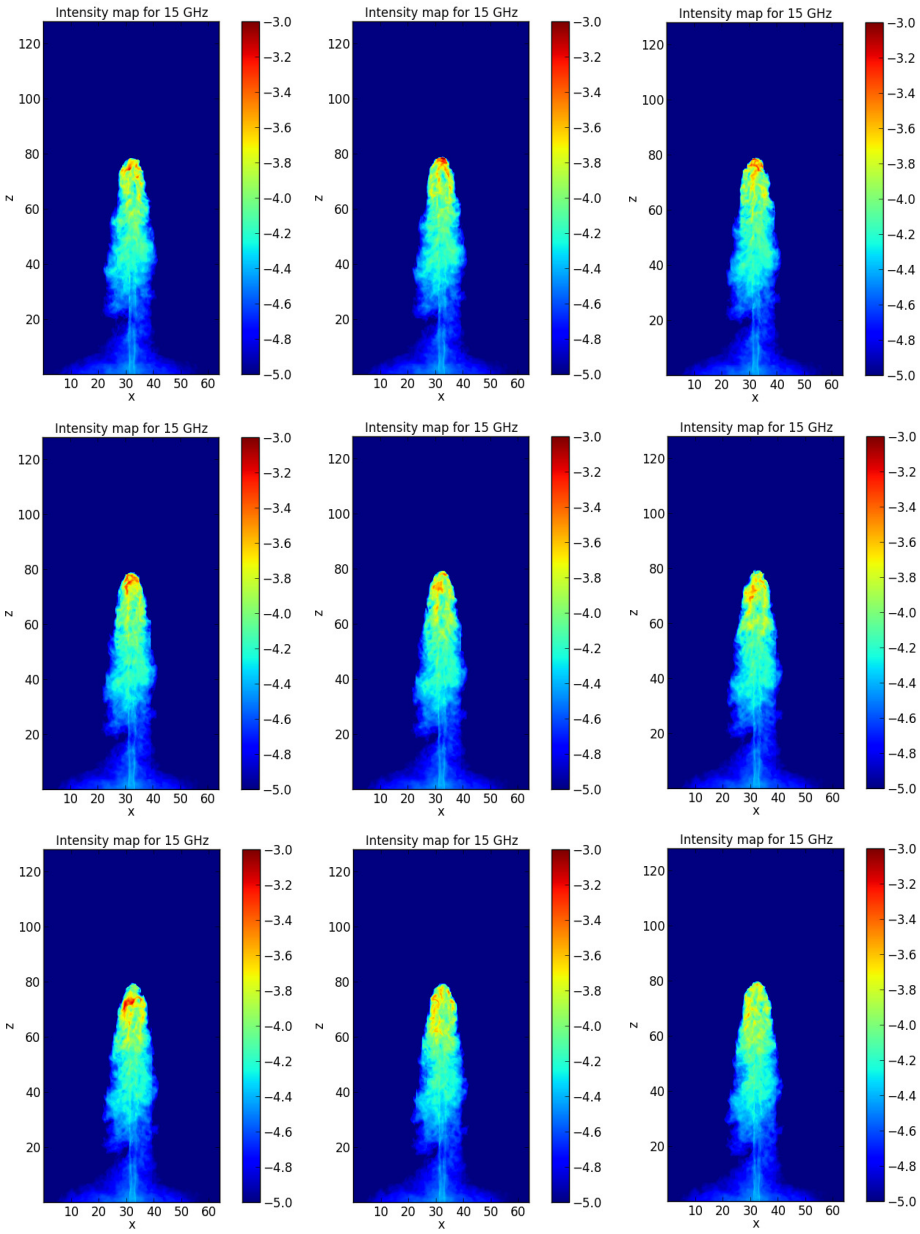

Figure 4: Intensity maps calculated at 15 GHz for sequential time steps

References

[1] G. Ghisellini *Radiative Processes in High Energy Astrophysics, volume 873 of Lecture Notes in Physics*, Berlin, Springer Verlag 2013

[2] M. Böttcher *Modeling the spectral energy distributions and variability of blazars*, *2011 Fermi & Jansky: Our Evolving Understanding of AGN* (preprint arXiv:1205.0539) 2011.

[3] M. L. Lister *et al. MOJAVE: Monitoring of jets in active galactic nuclei with VLBA experiments. V. Multi-epoch VLBA images*, *ApJ* **137** , 3718-3729, 2009.

[4] K.I. Kellermann, *et al. Sub-Milliarcsecond Imaging of Quasars and Active Galactic Nuclei. III. Kinematics of Parsec-scale Radio Jets*, *ApJ* **609**, 539-563, 2004.

[5] B. G. Piner, M. Mahmud, A. L. Fey, and K. Gospodinov *Relativistic jets in The Radio Reference Frame Image Database I: Apparent speeds from the first five years of data*, *ApJ* **133**, 2357-2388, 2007.

[6] A. Mignone, P. Rossi, G. Bodo, A. Ferrari, S. Massaglia *High-resolution 3D relativistic MHD simulations of jets*, *MNRAS* **402**, 7-12, 2010.

[7] P. Mimica, M. A. Aloy, E. Müller *Internal shocks in relativistic outflows: collisions of magnetized shells*, *A& A* **466** 93-106, 2007.

[8] P. Rossi, A. Mignone, G. Bodo, S. Massaglia and A. Ferrari *Formation of dynamical structures in relativistic jets: the FRI case*, *A&A* **488**, 795-806, 2008.

[9] P. Mimica, M. A. Aloy, I. Agudo, J. M. Marti, J. L. Gómez, J. A. Miralles *Spectral evolution of superluminal components in parsec-scale jets*, *ApJ* **696**, 1142-1163, 2009.

[10] A. Mignone, G. Bodo, S. Massaglia, T. Matsakos, O. Tesileanu, C. Zanni and A. Ferrari *PLUTO: a numerical code for computational astrophysics*, *ApJ* **170**, 228-42, 2007.

[11] E. F. Toro *Riemann Solvers and Numerical Methods for Fluid Dynamics: A Practical Introduction Third Edition*, Springer, Berlin, Chapter 1, pp 1-40, 2009.

[12] A. Mignone and G. Bodo *An HLLC Riemann solver for relativistic flows - II. Magnetohydrodynamics*, *MNRAS* **368**, 1040-1054, 2006.

[13] M. Böttcher, D. E. Harris and H. Krawczynski *Relativistic Jets from Active Galactic Nuclei*, Wiley-VCH Verlag GmbH & Co. KGaA, Weinheim, Germany, Chapter 3, pp 39-80, 2012.

[14] J. L. Gomez, J. M. Marti, A. P. Marscher, J. M. Ibáñez and J. M. Marcaide *Parsec-scale synchrotron emission from hydrodynamic relativistic jets in active galactic nuclei*, *ApJ* **449**, 19-21, 1995.

[15] J. M. Marti, E. Müller, J. A. Font, J. M. Ibáñez and Marquina *Morphology and dynamics of relativistic jets*, *ApJ* **479**, 151-163, 1997.

[16] M. Böttcher and C. Dermer *Timing signatures of the internal-shock model for blazars*, *ApJ* **711**, 445-460, 2010.